Journal of Inclusion Phenomena and Macrocyclic Chemistry **49**: 37–46, 2004.

An Improved Force Field for O_2, CO and CN Binding to Metalloporphyrins

FRANCISCO TORRENS
Institut Universitari de Ciència Molecular, Universitat de València, Dr. Moliner 50, E-46100 Burjassot (València), Spain, E-mail: Francisco.Torrens@uv.es

(Received: 10 December 2003; in final form: 16 December 2003)

Key words: CO/O_2 discrimination, electron-pair repulsion, iron–porphyrin complex, oxygen fixation, polarizing molecular mechanics

Abstract

Parametrization of a molecular-mechanics program to include terms specific for five- and six-coordinate transition metal complexes is applied to heme complexes. The principal new feature peculiar to five and six coordination is a term that represents the effect of electron-pair repulsion modified by the ligand electronegativity and takes into account the different possible structures of complexes. The model system takes into account the structural differences of the fixing centre in the haemoglobin subunits. The customary proximal histidine is added. The macrocycle heme IX is wholly considered in our model. The calculations show clearly that certain conformations of heme IX–histidine models are much more favourable than others for fixing O_2. From the O_2 binding in haemoglobin and myoglobin and in simple Fe porphyrin models it is concluded that the bent O_2 ligand is best viewed as bound superoxide, O_2^-. Rotation of axial ligands are practically free. A small modification of the model in both crystal and protein matrix affects the orientation of the ligands in experimental systems.

Abbreviations: AM1 – Austin Model 1; CO – carbon monoxide; DFT – density functional theory; EPR – electron-pair repulsion; Hb – haemoglobin; His – histidine; ID – interacting induced-dipole; Im – imidazole; LDA – local density approximation; Mb – myoglobin; mdi – malondialdiminate; MM – molecular mechanics; NID – non –interacting induced-dipole; O_2 – oxygen; P – porphyrin; Piv_2C_8 – α,α,5,15-[2,2′–(octanediamido)diphenyl]-α,α,10,20–bis(*o*-pivalamidophenyl)porphyrin; QM – quantum mechanics; TTP – *meso*-tetraphenylporphyrin.

Introduction

The heme group is in the active centre of a number of relevant proteins as the oxygen (O_2) transport proteins haemoglobin (Hb) and myoglobin (Mb) [1, 2], as well as enzymes involved in catabolism as peroxidases [3], catalases, oxidases [4] and cytochromes [5]. The replacement of Fe by Mg in heme leads to chlorophyll [6], and the replacement of Fe by other transition metals coupled with modifications in the aromatic ring leads to species as vitamin B_{12} [7] and cofactor F-430 [8]. The study of heme models is a focal point of experimental bioinorganic chemistry [9].

Rohmer and co-workers characterized the electronic state of Fe(P) (P = porphyrin) complexes [10–12], and predicted an electronic structure, which was later proved by experiment [13]. Other theoretical studies are devoted to the real position of the CO group in Fe(P)(Im)(CO) (Im = imidazole) complexes [14, 15], the position of the CN group in $Fe(mdi)_2(py)(CN)$ (mdi = malondialdiminate) complexes [16], the role of histidine (His)-distal and -proximal on the binding of O_2 in Hb [17–20], and structural aspects of the binding of O_2 and other ligands to heme [21–27]. The amount of information obtained from the quantum mechanical calculations is seriously limited by the size of the heme group itself, which has allowed only recently the appearance of theoretical studies on reactivity [28–33].

The coordination of O_2 to the Fe(P)(Im) 5-coordinate species leads to 6-coordinate species with octahedral geometry, i.e., the biomimetic forms of Mb—O_2 and Hb—O_2. X-ray data were reported only on two complexes, $Fe(T_{piv}PP)$[1-(Me)Im](O_2) [34] and $Fe(T_{piv}PP)$[2-(Me)Im](O_2) [35]. Both complexes are quite similar, sharing the same porphyrin $T_{piv}PP$, which is *meso*-tetrakis(α,α,α,α-*o*-pivalamidophenyl)porphyrin. Maseras and co-workers optimized the geometry of $Fe(T_{piv}PP)$[1-(Me)Im](O_2) with the hybrid quantum mechanics/molecular mechanics (QM/MM) method IMOMM (DFT-B3LYP basis set double-ζ(d):MM3) [36] and pure QM DFT-B3LYP basis set 6-31G(d) [37]. Ghosh and Bocian optimized the geometry of Fe(P)(Im)(CO) with density functional theory (DFT) basis set double-ζ + polari-zation [19]. Salzmann *et al.* optimized under constraint the geometry of a $Fe(T_{piv}PP)$[1-(Me)Im](CO) model with DFT-B3LYP Watchers' 62111111/331211/

3111/3 basis set [38]. Han *et al.* calculated a heme model–CO system employing the *ab initio* pseudopotential method with local density approximation (LDA) exchange correlation (unpublished basis set) [39].

The reversible binding of O_2 and carbon monoxide (CO) played a central role in studies of heme-protein structure and function. Numerous encumbered Fe^{II} porphyrin models were synthesized in an effort to elucidate the structural details of small ligand binding. The steric bulk of certain axial ligands bonded to synthetic Fe^{II} porphyrins provided model compounds of reduced O_2 and CO affinity, and models of the so-called tense (T) state of hemoproteins. Unfortunately, thus far there is only one single-crystal X-ray structure determination on such a complex [40]. There was much discussion on the mechanistic basis of the variation of affinity values in heme proteins and model compounds. This focused on the nature of the axial ligand, distal steric effects, distal polar effects, and enforced doming and ruffling of the porphyrin skeleton. Johansson *et al.* showed by quantum chemical calculations on a haem *a* model that upon reduction the spin pairing at Fe is accompanied by effective delocalization of electrons from the Fe towards the periphery of the porphyrin ring, including its substituents [41, 42].

In previous papers [43, 44], both non-interacting (NID) and interacting (ID) induced-dipole polarization models were implemented in the program molecular mechanics (MM2) [45]. The polarizing force field for proteins (MMID2) was described elsewhere [43] and applied to *N*-formylglycinamide (For-Gly-NH_2) [44]. MMID2 was improved to include terms specific for five- and six-coordination [46]. The new program is called MMIDX. In this study a new force field for O_2, CO and CN binding to metalloporphyrins has been tested. The next section presents the computational method. Following that, the improvements in the force field are described. Next, the calculation results are discussed. Finally, the conclusions are summarized.

Computational method

The electric polarization energy E^{pol} is the energy required to make the induced dipoles,

$$E^{\mathrm{pol}} = \sum_{p=1}^{N} E_p^{\mathrm{pol}} = -\frac{1}{2}\sum_{p=1}^{N} \frac{\mu_p \cdot \mu_p}{\alpha_p}, \tag{1}$$

where N is the number of atoms. The procedure by non-interacting induced dipoles (NID) assumes scalar isotropic point (atomic) polarizabilities. Since the electric field at each position must be evaluated to determine the induced dipoles, E_{pol} is most easily evaluated from this field,

$$E^{\mathrm{pol}} = -\frac{1}{2}\sum_{p=1}^{N} \alpha_p \mathbf{E}_p \cdot \mathbf{E}_p. \tag{2}$$

On the other hand, the procedure by interacting induced dipoles (ID) allows the interaction of the induced dipole moments by means of tensor effective anisotropic point polarizabilities. The molecular polarizability, $\alpha_{\alpha\beta}^{\mathrm{mol}}$, is defined as the linear response to an external field,

$$\mu_\alpha^{\mathrm{ind}} = \alpha_{\alpha\beta}^{\mathrm{mol}} E_\beta^{\mathrm{ext}}, \tag{3}$$

where $\mu_\alpha^{\mathrm{ind}}$ is the induced molecular dipole moment. Considering a set of N polarizable interacting atoms, the atomic induced dipole moment has a contribution also from the other atoms,

$$\mu_{p,\alpha}^{\mathrm{ind}} = \alpha_{p,\alpha\beta}\left(E_\beta^{\mathrm{ext}} + \sum_{q\neq p}^{N} T_{pq,\beta\gamma}^{(2)} \mu_{q,\gamma}^{\mathrm{ind}}\right), \tag{4}$$

where $T_{pq,\beta\gamma}^{(2)}$ is the interaction tensor as modified by Thole [47]

$$T_{pq,\alpha\beta}^{(2)} \frac{3v_{pq}^4 r_{pq,\alpha} r_{pq,\beta}}{r_{pq}^5} - \frac{(4v_{pq}^3 - 3v_{pq}^3)\delta_{\alpha\beta}}{r_{pq}^3}, \tag{5}$$

where $v_{pq} = r_{pq}/s_{pq}$ if $r_{pq} < s_{pq}$; otherwise $v_{pq} = 1$. s is defined as $(\Phi_p \Phi_q)^{1/4}$, where Φ_p is a fitting parameter proportional to the atomic second-order moment. Molecular polarizability can be written as

$$\alpha_{\alpha\beta}^{\mathrm{mol}} = \sum_{q,p}^{N} \mathbf{B}_{pq,\alpha\beta}, \tag{6}$$

where $\mathbf{B}$ is the relay matrix defined from atomic α-s as (in a supermatrix notation)

$$\mathbf{B} = (\alpha^{-1} - T^{(2)})^{-1}. \tag{7}$$

Force-field modifications

1,3-interactions between atoms bonded to a common atom are not specifically included in Equation (8) in the MM2 + polarization approach because they are effectively already included in the bond-length and bond-angle *strainless* parameters.

$$E_{\mathrm{steric}} = \sum E_{\mathrm{str}} + \sum E_{\mathrm{bend}} + \sum E_{\mathrm{tors}} + \sum E_{\mathrm{nb}}. \tag{8}$$

However, for 5-coordinate structures, there is a need to consider the effect of 1,3-interactions because an energy term is needed for ligand–ligand repulsion to account for (1) the stability difference of various geometries possible, and (2) structural effects due to the variation of ligand electronegativity. Since the geometries of the methylfluorophosphoranes $(CH_3)_n PF_{5-n}$ $(n = 0 \rightarrow 3)$ were qualitatively correlated with Gillespie's VSEPR theory, VSEPR was adopted as a model for the present

approach. Bond electron-pair repulsion (EPR) terms were introduced *via* the non-bonded term E_{nb} of Equation (6) modified to express EPR for atoms bonded to 5- or 6-coordinated atoms. The unmodified term is

$$E_{\mathrm{nb}(AB)} = \varepsilon\left[8.28 \cdot 10^5 \exp\left(-\frac{1}{0.0736P}\right) - 2.25P^6\right], \tag{9}$$

where $P = [r_{\mathrm{VDW}(A)} + r_{\mathrm{VDW}(B)}]/r_{AB}$, r_{VDW} is the van der Waals radius of the specific atom, and r_{AB} is the non-bonded distance between A and B; $\varepsilon = (\varepsilon_A\varepsilon_B)^{1/2}$ where ε_A and ε_B are parameters specific to atoms A and B, and are related to the hardness of the atoms. Hill evaluated the constants in Equation (9), which give the energy $E_{\mathrm{nb}(AB)}$ in units of kilocalories per mole [48].

The modification of Equation (7) to express 1,3-bond EPR terms is [49]

$$E_{(1,3)AB} = D \cdot \varepsilon\left[8.28 \cdot 10^5 \exp\left(-\frac{1}{0.0736P^*}\right) - 2.25P^{*6}\right]. \tag{10}$$

The addition of a scaling factor D, to obtain a suitable balance between this term and the other terms in Equation (6), and the replacement of P with P^* (where $P^* = [r_{\mathrm{VDW}(A)} + r_{\mathrm{VDW}(B)}]/r^*_{AB}$ and r^*_{AB} is the distance between atoms A and B calculated from modified bond lengths, d^*_{CA} and d^*_{CB}, between the central atom C and either atom A or B) provide the necessary adjustments to quantitatively reproduce the $(CH_3)_nPF_{5-n}$ structures [50]. The variation in ligand electronegativity is introduced by a distance factor R_A in the relation $d^*_{CA} = d_{CA}R_A$. The magnitude of R is inversely related to the electronegativity difference between atoms C and A. The R factors are the means of including the concept of EPR between atoms A and B. If the electronegativity difference ΔX_{CA} is large, the bonding electron pair can be considered to move away from atom C, thus decreasing EPR between C—A and C—B bonds. When $\Delta X_{CA} > \Delta X_{CA'}$, the repulsion term $E_{(1,3)AB} < E_{(1,3)A'B}$ even when the actual bond lengths are equal. A set of distance factors R may be obtained from the bond ionic character I,

$$I = 1 - \exp\left[-\frac{1}{4}(\Delta X_{CA})^2\right] \tag{11}$$

and using the relation

$$R = \frac{I \cdot r_A + r_C}{r_A + r_C}, \tag{12}$$

where r_A and r_C are covalent radii of atoms A and C.

Description of program POLAR

POLAR calculates molecular electric charges and polarizablities [51]. Describing the partial charge method developed for the Mulliken scale [52], Huheey mentioned that most elements double their electronegativities as the partial charge approaches +1 whereas their electronegativities essentially disappear as the partial charge approaches −1 [53]. The Mulliken and Pauling scales are roughly proportional, so Huheey's observation may be expressed in Pauling units as $X_{\mathrm{eq}} = X_A + \Delta_A X_A$. Here, X_{eq} is the electronegativity as equalized through Sanderson's principle, X_A is the initial, pre-bonded electronegativity of a particular atom A and Δ_A is the σ partial charge on A [54]. Charge conservation leads to a general expression for $X_{\mathrm{eq}} = (N+q)/(\Sigma_{\mathrm{atoms}}v_A/X_A)$, where $N = \Sigma v$ equals the total number of atoms in the species formula and q is the σ molecular charge. The σ partial charge Δ_A on atom A can be generalized as $\Delta_A = \Sigma_{\mathrm{bonds}}(X_{\mathrm{eq},b} - X_A)/X_A$ and the electronegativity equalized for bonds is given as $X_{\mathrm{eq},b} = (2+q/m)/(1/X_A + 1/X_B)$, where m is the number of bonds in the molecule. π-net charges and polarizabilities have been evaluated with the Hückel molecular orbital (HMO) method. HMO β parameter can be evaluated, in first approximation, between p_z orbitals twisted from co-planarity by an angle θ as $\beta = \beta_0 \cos\theta$, where β_0 is equal to the β parameter for benzene [55]. The electronic coupling V_{ab} of the binuclear mixed-valence M^{II}–L–M^{III} complex $[(NH_3)_5$-Ru-bipyridyl-Ru$(NH_3)_5]^{5+}$ showed that when a pyridine ring rotates, π–$\pi V_{ab}(\theta)$ can be best fitted by $\cos^{1.15}\theta$ [56]. The β function is assumed universal:

$$\beta = \beta_0 \cos^{1.15}\theta. \tag{13}$$

The dipole and tensor quadrupole moments have been calculated from the point distribution of net charges. The dipole moment vector is calculated as

$$\mu_a = \sum_i q^i r^i_a, \tag{14}$$

where q^{i} is the ith element of charge at the point $\mathbf{r}^{\mathrm{i}}$ relative to an origin fixed at the centre of mass. The subscripts a, b,..., denote the Cartesian components. Only the first, nonvanishing moment is independent of the choice of origin. Thus for an ion like OH^-, μ varies with the origin. In order to avoid this dependence, the origin is taken at the centre of mass and the molecule is brought into its principal internal coordinate system.

Sanderson's principle allows the calculation of the σ atomic polarizability as:

$$\alpha_A = \frac{\partial\Delta_A}{\partial X_A} = \sum_{\mathrm{bonds}} \frac{f_A s_A (1-\Delta_A)\left(2-\frac{q}{m}\right)X_B}{(2-\Delta_A-\Delta_B)(X_A+X_B)^2}, \tag{15}$$

where the coefficients f_A and s_A have been introduced to take into account the effects of the atomic charge (Δ_A), internal sub-shells and lone pairs on α_A. f_A and s_A are calculated as $f_A = 1 - 1.5\Delta_A + 0.5\Delta_A^2$ and $s_A = C_A + 0.15L_A$, where C_A is related to the number of internal sub-shells and L_{A} is the number of lone pairs on

atom A. The σ atomic polarizability tensors are calculated as:

$$\alpha_\sigma = \sum_{\text{bonds}} \frac{3\alpha_\sigma}{\alpha^{\parallel} + 2\alpha^{\perp}} \begin{bmatrix} \alpha^{\perp} & 0 & 0 \\ 0 & \alpha^{\perp} & 0 \\ 0 & 0 & \alpha^{\parallel} \end{bmatrix} = \sum_{\text{bonds}} \frac{3\alpha_\sigma}{3.676} \begin{bmatrix} 1 & 0 & 0 \\ 0 & 1 & 0 \\ 0 & 0 & 1.676 \end{bmatrix}, \quad (16)$$

where the z-axis is along the bond direction for each bond. The diagonal form of α_σ has two components: $\alpha^{\parallel}$ and $\alpha^{\perp}$, parallel and perpendicular, respectively, to the bond axis. Parameter $\alpha^{\parallel}/\alpha^{\perp} = 1.676$ has been obtained fitting the bonding polarizabilities of Vogel [57] implemented in the database of program SIBFA [58]. The π atomic polarizability tensor is calculated as:

$$\alpha_\pi = \sum_{\text{bonds}} \frac{3\alpha_\pi}{2\alpha^{\parallel} + \alpha^{\perp}} \begin{bmatrix} \alpha^{\parallel} & 0 & 0 \\ 0 & \alpha^{\parallel} & 0 \\ 0 & 0 & \alpha^{\perp} \end{bmatrix} = \sum_{\text{bonds}} \frac{3\alpha_\pi}{3.741} \begin{bmatrix} 1 & 0 & 0 \\ 0 & 1 & 0 \\ 0 & 0 & 1.741 \end{bmatrix}, \quad (17)$$

where the xy plane is the σ-plane. $\alpha^{||}$ and $\alpha^{\perp}$ are parallel and perpendicular to the σ-plane. Parameter $\alpha^{\perp}/\alpha^{||} = 1.741$ has been obtained by fitting the experimental polarizabilities of aromatic molecules.

Calculation results and discussion

In a previous report [46] the MMX + polarization force field was applied to the binding of O_2, CO and CN to metalloporphyrins with an EPR parameter of $D = 0.2$. In the present paper a comparative study is presented with $D = 0.1$. The structure of the heme(—His)—O_2 model is shown in Figure 1. Heme is the prosthetic group of Hb. The molecular mechanics calculations use the MM2/MMX + polarization force fields. The van der Waals parameters for the Fe atom have been taken from the UFF force field [59], and the torsional contributions involving dihedral angles with the metal atom and the bending terms involving Fe in central position have been set to zero.

The molecular mechanics dipole moment of the heme IX models is collected in Table 1. In general, the dipole moment increases with the oxidation state of Fe. In particular, the dipole moment of the Fe^{III} heme(—His)—CN results the greatest due to the polar $Fe^{\delta+}$—C—$N^{\delta-}$ complex. The dipole moment of the Fe^{III} heme(—His)—O_2 is relatively large, due to the polar $Fe^{\delta+}$—O—$O^{\delta-}$ complex. In general, the inclusion of polarization in MM2 corrects the dipole moment in the correct direction when compared with MMX + ID. In particular, for heme(—His) the MM2 + polarization dipole moment remains almost constant. The binding of His in heme increases the dipole moment by a factor of 6. Moreover, the binding of CN in heme—His increases the dipole moment by 83%. However, the binding of O_2 or CO decreases the dipole moment by only 1–7%.

The 4-coordinate Fe(P) system

The heme group has little direct application in biochemistry, but it is a natural starting point for both experimental and theoretical studies. The crystal structures of a number of heme derivatives were reported, with different substituents in the ring [13]. The simplest

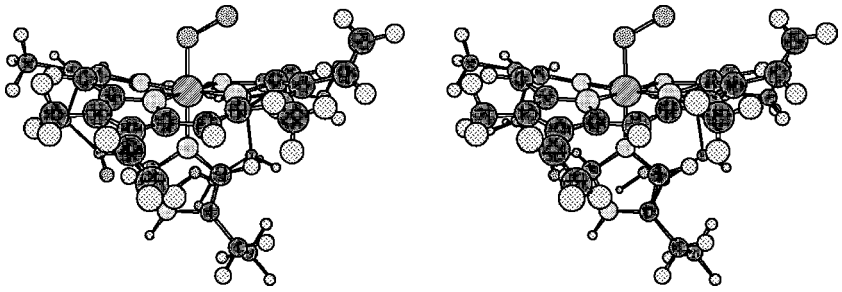

Figure 1. Stereo view of the heme(—His)—O_2 model. Heme is the prosthetic group of haemoglobin.

Table 1. Molecular mechanics (MMX) results for heme-IX adduct models: dipole moments in debyes

Adduct	Fe oxidation state	MM2	MM2 + NID[a]	MM2 + ID[b]	MMX	MMX + NID[a]	MMX + ID[b]
Heme	2	0.467	0.483	0.539	0.467	0.483	0.539
Heme(—His)	2	2.840	2.725	2.819	2.515	2.974	3.795
Heme(—His)—O_2	3	2.512	2.372	3.091	3.458	2.542	3.187
Heme(—His)—CO	2	2.723	2.725	2.905	3.252	1.878	2.567
Heme(—His)—CN	3	5.090	5.538	5.470	5.031	5.247	5.534

[a] NID: polarization by non-interacting induced dipoles; [b] ID: polarization by interacting induced dipoles.

Table 2. Selected geometric parameters (Å and degrees) from the geometry optimization of Fe(P) with the pure B3LYP and with the IMOMM(B3LYP:MM3) methods [37][a]

Parameter	MM2	MM2 + NID[b]	MM2 + ID[c]	MMX[d]	MMX[d] + NID[b]	MMX[d] + ID[c]
Fe—N[e]	1.881	1.878	1.877	1.881	1.878	1.877
N—C	1.353	1.352	1.350	1.353	1.352	1.350
$C—C_{bridge}$	1.337	1.336	1.334	1.337	1.336	1.334
C—C′	1.341	1.340	1.339	1.341	1.340	1.339
C′—C″	1.332	1.332	1.332	1.332	1.332	1.332
Fe—N—C	128.6	128.6	128.6	128.6	128.6	128.6
N—Fe—N	90.2	90.2	90.2	90.2	90.2	90.2
$N—C—C_{bridge}$	120.8	120.8	120.9	120.8	120.8	120.9
N—C—C′	112.0	112.1	112.1	112.0	112.1	112.1
Parameter	Experiment	Pure QM	QM/MM			
Fe—N	1.966	2.016	1.940			
N—C	1.378[e]	1.397	1.362			
$C—C_{bridge}$	1.395[e]	1.402	1.369			
C—C′	1.439[e]	1.459	1.345			
C′—C″	1.365[e]	1.367	1.333			
Fe—N—C	127.2[e]	127.4	127.7			
N—Fe—N	90.0[e]	90.0	90.0			
$N—C—C_{bridge}$	125.3[e]	125.5	126.2			
N—C—C′	110.6[e]	110.4	110.3			

[a] Experimental data on the Fe(TPP) system are also provided for comparison [13]; [b] NID: polarization by non-interacting induced dipoles; [c] ID: polarization by interacting induced dipoles; [d] Scaling factor $D = 0.1$; [e] Average values.

model, with all substituents being H atoms, was not provided. Because of this, comparison will be made with a species containing some substituents. In particular, Fe(TPP) (TPP = *meso*-tetraphenylporphyrin) has been chosen [13]. Its electronic state is well known experimentally to correspond to a low spin triplet ($S = 1$). Selected structural parameters are collected in Table 2. The agreement in bond angles between both MM2/MMX + polarization geometries and the X-ray structure is good, with discrepancies always smaller than 5°. Differences in bond distances are larger in a number of cases. This is the case of the $C—C_{bridge}$, C—C′ and C′—C″ distances. These distances have values of 1.395, 1.439 and 1.365 Å, respectively, in X-ray, ca. 1.336, 1.340 and 1.332 Å, respectively, in MM2/MMX + po-polarization. Agreement between experiment and MM2/MMX + polarization is good (ca. 0.06 Å). All these atoms are in part purely described with MM2, and the optimized MM2/MMX + polarization values are close to the optimal bond distance for these types of atoms in the applied force field, which is 1.337 Å. Another discrepancy in the geometries appears in the Fe—N distance. This is more puzzling, because the calculated distance 1.877–1.881 Å is smaller than the experimental value of 1.966 Å.

The 5-coordinate Fe(P)(Im) system

Coordination of an Im ligand to the heme group leads to a 5-coordinate species with a square pyramidal geometry. These compounds are good biomimetic models of both Mb and Hb, Im replacing His-proximal of the biological systems. The need to avoid both dimerization and formation of 6-coordinate species with two axial ligands poses serious restrictions on the nature of the porphyrins able to give this kind of complexes. For this study, the species Fe(Piv_2C_8)[1-(Me)Im] {Piv_2C_8 = α,α,5,15-[2,2′-(octanediamido)diphenyl]-α,α,10,20-bis(*o*-pivalamidophenyl)porphyrin} has been chosen. This species has the advantage of having 1-methylimidazole as axial ligand, in constrast with the more common 2-methylimidazole, which is more sterically demanding. Unfortunately, neither for Fe(Piv_2C_8)[1-(Me)Im] nor for other 5-coordinate derivatives of heme the electronic state is experimentally known. Electronic spectroscopy, magnetic susceptibility and Mössbauer measurements are conclusive in identifying it as high spin ($S = 2$). Selected parameters are resumed in Table 3. The $Fe—N_{porphyrin}$ distances are longer by ca. 0.05 Å (MMX + ID) than those in the 4-coordinate system. This trend is in agreement with the reference values. The result is fully consistent with the shift from low spin to high spin in the metal. The present result improves the previous study [46], which presented these distances longer by 0.06 Å. Most data focus on the description of Im. Overall agreement in the geometric parameters is correct. Moreover, one has to take with suspicion the X-ray parameters of Im, which would make the N=C double bond $N_{Im}—C_{Im}$ of Im longer than the N—C single bond $N_{Im}—C'_{Im}$. However the MM calculations are, in general, in agreement with the QM/MM reference, which provides the expected result.

The sharper discrepancy concerns the $N_{porphyrin}—Fe—N_{Im}—C_{Im}$ dihedral angle. This angle measures the rotation around the $Fe—N_{Im}$ single bond, and rules the placement of the Im plane with respect to the

Table 3. Selected geometric parameters (Å and degrees) from the geometry optimization of Fe(P)(NH=CH_2) with the pure B3LYP and of Fe(P)[1-(Me)Im] with the IMOMM(B3LYP:MM3) methods [37][a]

Parameter	MM2	MM2 + NID[b]	MM2 + ID[c]	MMX[d]	MMX[d] + NID[b]	MMX[d] + ID[c]
Fe—$N^{e}_{porphyrin}$	1.897	1.894	1.890	1.921	1.904	1.923
Fe—N_{Im}	1.866	1.863	1.864	2.003	1.936	2.015
N_{Im}—C_{Im}	1.327	1.327	1.326	1.438	1.449	1.436
N_{Im}—C'_{Im}	1.344	1.343	1.338	1.464	1.442	1.412
Fe—N_{Im}—C_{Im}	126.3	126.3	126.1	122.1	143.7	151.0
Fe—N_{Im}—C'_{Im}	126.7	126.6	126.3	142.2	112.5	122.4
$N_{porphyrin}$—Fe—N_{Im}—C_{Im}	115.8	115.7	114.9	162.0	103.5	138.4

Parameter	Experiment	Pure QM	QM/MM
Fe—$N_{porphyrin}$	2.074	2.101	2.029
Fe—N_{Im}	2.134	2.252	2.233
N_{Im}—C_{Im}	1.350	1.279	1.299
N_{Im}—C'_{Im}	1.250	–[f]	1.414[g]
Fe—N_{Im}—C_{Im}	127.0	126.1	136.8
Fe—N_{Im}—C'_{Im}	120.0	120.6	122.6
$N_{porphyrin}$—Fe—N_{Im}—C_{Im}	126.0	90.0	133.2

[a] Experimental data on the Fe(Piv_2C_8)[1-(Me)Im] system are also provided for comparison [60]; [b] NID: polarization by non-interacting induced dipoles; [c] ID: polarization by interacting induced dipoles; [d] Scaling factor $D = 0.1$; [e] Average values; [f] Frozen in calculation; [g] Corresponds to N—H in this calculation.

porphyrin ring. Its sign is arbitrary because the x and y directions are equivalent in absence of axial ligand. In this work, a positive sign has been chosen for consistence with data on the 6-coordinate complexes presented below. An angle of 90° (like in the pure QM reference) means that the Im plane is eclipsing one of the Fe—$N_{porphyrin}$ bonds, while an angle of 135° (≈133.2° in QM/MM) indicates a staggered orientation of Im with respect to the Fe—$N_{porphyrin}$ bonds. Therefore, both pure QM and QM/MM values are just opposite with the experimental value (126.0°) lying in between, although closer to the QM/MM value. The structural minima lead to structures where the Im ligand is located about the bisector of an angle $N_{porphyrin}$—Fe—$N_{porphyrin}$. The MMX + polarization results lie, in general, in the range 90°–133° of the references. The importance of the large discrepancy between different values is, however, arguable, because there is also a large dispersion in different experimental 5-coordinate derivatives of heme, as well as in experimental reports of both Mb and Hb. It seems, therefore, that the rotation around this single bond has a very low barrier.

The 6-coordinate Fe(P)(Im)(O_2) system

Coordination of O_2 to the 5-coordinate heme—His species leads to 6-coordinate species with an octahedral geometry. These compounds are the biomimetic forms of Mb—O_2 and Hb—O_2. X-ray data are reported only on two complexes, Fe(T_{piv}PP)[1-(Me)Im](O_2) and Fe(T_{piv}PP)[2-(Me)Im](O_2). Both complexes are quite similar, sharing the same porphyrin T_{piv}PP, which is *meso*-tetrakis(α,α,α,α-*o*-pivalamidophenyl)porphyrin. The Fe(T_{piv}PP)[1-(Me)Im](O_2) complex, containing the less sterically demanding 1-methylimidazole ligand, has been chosen for comparison. The state of this system is a low spin open-shell singlet ($S = 1$) resulting in a Fe^{III}—O_2^- charge distribution. Selected parameters are reported in Table 4. The parameters concerning the coordination of O_2, which are probably the most critical for the biochemical activity of Hb, are well reproduced. The computed values for the Fe—O distance, 1.8–1.9 Å, are close to the experimental value of 1.746 Å. The calculated values (1.21–1.30 Å) for the O—O distance are far from the experimental report of 1.163 Å. However, the experimental value (even shorter than the 1.21 Å for free O_2) is suspect, because of the disorder on the placement of the second O atom within the crystal, as admitted by the authors of the X-ray experiment themselves [34]. The O—O interatomic distance increases from 1.21 Å in free O_2 to 1.298 Å (MMX + ID), suggesting that electronic charge is transferred from FeP to O_2, in agreement with the experimental result that the Fe—O_2 bond can be formally described as Fe^{III}—O_2^- [9].

The most significant feature of the present structure is the bent Fe—O—O bond. The Fe—O—O bond angles are in all cases indicative of a bent η^1 coordination mode, where only one O atom is directly attached to the metal. These calculations are in agreement with the experiment and calculation references. Atomic net charges have been calculated with our program POLAR. The results, $q_{Fe} = 3.078$, $q_{O(Fe)} = -0.412$ and $q_{O(O)} = -0.531$e are in agreement with Weiss' model for the Fe—O_2 bond in which the bond might be ionic between a Fe^{3+} and a superoxide ion, net charge being transferred from Fe to O_2 ($Fe^{3+}O_2^-$) [61]. Experimental support for Weiss' model was first advanced by Misra and Fridovich [62]. The geometry agrees with Pauling's prediction of a bent FeO_2 bond, and the O—O distance

Table 4. Selected geometric parameters (Å and degrees) from the geometry optimization of Fe(P)(NH=CH_2)(O_2) with the pure B3LYP and of Fe(P)[1-(Me)Im](O_2) with the IMOMM(B3LYP:MM3) methods [37], and of Fe(T_{piv}PP)(Im)(O_2) with LSD [21][a]

Parameter	MM2	MM2 + NID[b]	MM2 + ID[c]	MMX[d]	MMX[d] + NID[b]	MMX[d] + ID[c]
Fe—$N^{e}_{porphyrin}$	1.880	1.876	1.870	1.923	1.925	1.909
Fe—N_{Im}	1.871	1.862	1.861	2.020	1.990	1.996
Fe—O	1.847	1.841	1.845	1.890	1.875	1.910
O—O	1.211	1.210	1.210	1.279	1.269	1.298
Fe—O—O	123.5	121.5	122.8	120.1	143.9	125.8
O—Fe—N_{Im}	171.7	169.5	168.6	139.1	129.0	136.5
$N_{porphyrin}$—Fe—N_{Im}—C_{Im}	179.0	178.2	176.8	170.4	170.2	173.4
$N_{porphyrin}$—Fe—O—O	−3.3	−5.0	−16.5	−36.7	−29.0	−21.1
Parameter	Experiment	Pure QM		QM/MM		LSD
Fe—$N_{porphyrin}$	1.978	2.035		1.949		2.010
Fe—N_{Im}	2.070	2.050		2.167		2.070[f]
Fe—O	1.746	1.757		1.759		1.770
O—O	1.163	1.268		1.286		1.300
Fe—O—O	129.4	121.1		117.0		121.0
O—Fe—N_{Im}	180.0	175.8		179.4		–
$N_{porphyrin}$—Fe—N_{Im}—C_{Im}	159.5	177.9		137.0		–
$N_{porphyrin}$—Fe—O—O	−42.4	−44.6		−44.1		–

[a] Experimental data on the Fe(T_{piv}PP)[1-(Me)Im](O_2) system are also provided for comparison [34]; [b] NID: polarization by non-interacting induced dipoles; [c] ID: polarization by interacting induced dipoles; [d] Scaling factor $D = 0.1$; [e] Average values; [f] Frozen in calculation.

is close to that of 1.27 Å, predicted by him [63]. It is slightly shorter than that of 1.34 Å in O_2^-, close to the electron spin resonance results, which show that no more than 2/3 of the density of one electron is transferred from the metal to the antibonding π^* orbitals of O_2.

The sharper discrepancy concerns the $N_{porphyrin}$—Fe—O—O dihedral angle. This angle measures the rotation around the Fe—O single bond, and rules the placement of the Fe—O—O plane with respect to the porphyrin ring. An angle of 0° (≈−3.3° in MM2) means that the Fe—O—O plane is eclipsing one of the Fe—$N_{porphyrin}$ bonds, while an angle of −45° (≈−44.6° in pure QM) indicates a staggered orientation of the O_2 with respect to the Fe—$N_{porphyrin}$ bonds. The structural minima lead to structures where the O_2 ligand is located about the bisector of an angle $N_{porphyrin}$—Fe—$N_{porphyrin}$. The MMX/MMX + NID results lie near the reference results. The present result (MMX + polarization mean angle of −29°) improves the previous study (mean angle of −24°) [46]. The structural minima correspond to a situation where the ending O of O_2 is placed above the opposite quadrant where the N'_{Im} is placed. This corresponds to a *trans* isomer.

The 6-coordinate Fe(P)(Im)(CO) system

Selected structural parameters of Fe(P)(Im)(CO) are shown in Table 5. The geometric parameters concerning the coordination of CO, which are probably the most critical for the biochemical activity of Hb, are well reproduced. The computed values for the Fe—C distance, 2.0–2.1 Å, are close to the experimental value of 1.793 Å. The calculated values (1.1–1.2 Å) for the C—O distance are close to the experimental report of 1.095 Å. The C—O interatomic distance is similar in the free molecule (1.171 Å, calculated with AM1 [64]) and 1.169 Å (MMX), suggesting that electronic charge is not transferred from FeP to CO. This is in agreement with the experimental result that the Fe—CO bond can be formally described as Fe^{II}—CO [9].

The most significant feature of the present structure is the linear Fe—C—O bond. While such a linear bond is to be expected based on the extensive literature on transition metal CO complexes, the result is nonetheless highly significant since bent Fe—C—O bonds with bond angles of 135°–145° appear to be the rule in various CO complexes of hemoproteins [65–67]. The global energy minimum is linear for Fe—C—O (MM2 + polarization, MMX and MMX + ID). These calculations are in agreement with the experiment and calculation references.

The rotation of the Im side chain is significant. The Im ring is rotated so that the N atom is directed toward the Fe atom, and the rotation angle $N_{porphyrin}$—Fe—N_{Im}—C_{Im} reaches ca. 176° (MM2 + polarization) in agreement with the LDA reference (174.2°). The present result (MMX + polarization mean angle of 172°) improves the previous study (mean angle of 155°) [46].

The 6-coordinate Fe(P)(Im)(CN) system

Selected bond lengths and angles are summarized in Table 6. The geometric parameters concerning the coor-

Table 5. Selected geometric parameters (Å and degrees) from the complete geometry optimization of Fe(P)(Im)(CO) with LDA [39], partial geometry optimization of Fe(T_{piv}PP)[1-(Me)Im](CO) with DFT (B3LYP and BPW91) [38], and complete geometry optimization of Fe(mdi)$_2$(py)(CO) with NLDFT [16], of Fe(P)(Im)(CO) with LDFT [19] and of Fe(T_{piv}PP)(Im)(CO) with LSD [21][a]

Parameter	MM2	MM2 + NID[b]	MM2 + ID[c]	MMX[d]	MMX[d] + NID[b]		MMX[d] + ID[c]
Fe—$N^{e}_{porphyrin}$	1.878	1.873	1.871	1.888	1.917		1.896
Fe—N_{Im}	1.868	1.863	1.862	1.947	2.043		1.977
Fe—C	1.971	1.970	1.970	2.050	2.118		2.048
C—O	1.110	1.109	1.110	1.169	1.166		1.166
Fe—C—O	180.0	180.0	180.0	176.1	167.9		176.9
C—Fe—N_{Im}	179.7	174.6	174.3	135.6	127.2		136.4
$N_{porphyrin}$—Fe—N_{Im}—C_{Im}	136.0	178.9	176.0	178.3	177.8		159.1
Parameter	Experiment	LDA	B3LYP	BPW91	NLDFT	LDFT	LSD
Fe—$N_{porphyrin}$	2.003	1.990	–	–	1.961	1.983	2.020
Fe—N_{Im}	2.071	1.960	–	–	2.139	1.966	2.070[f]
Fe—C	1.793	1.790	1.801	1.743	1.739	1.733	1.720
C—O	1.095	1.160	1.147	1.167	1.166	1.165	1.170
Fe—C—O	179.3	180.0	180.0	180.0	180.0	180.0	180.0
C—Fe—N_{Im}	178.3	180.0	180.0	180.0	180.0	180.0	–
$N_{porphyrin}$—Fe—N_{Im}—C_{Im}	–	174.2	–	–	–	–	–

[a] Experimental data on the Fe(T_{piv}PP)[1-(Me)Im](CO) system are also provided for comparison [38]; [b] NID: polarization by non-interacting induced dipoles; [c] ID: polarization by interacting induced dipoles; [d] Scaling factor $D = 0.1$; [e] Average values; [f] Frozen in calculation.

dination of CN are well reproduced. The computed values for the Fe—C distance, 1.9–2.1 Å, are in agreement with the experimental value of 1.930 Å. The calculated values (1.16–1.22 Å) for the C—N distance are close from the experimental report of 1.150 Å. The C—N interatomic distance increases from 1.147 Å (AM1) in the free molecule to 1.217 Å (MMX + NID), suggesting that electronic charge is transferred from FeP to CN. This is in agreement with the experimental result that the Fe—CN bond can be formally described as Fe^{III}— $(CN)^{-}$ [9].

The most significant feature of the present structure is the linear Fe—C—N bond. The global energy minimum is linear for Fe—C—N (MM2/MMX + polarization). These calculations are in agreement with the experiment and calculation references and with the previous study [46].

Conclusions

From the preceding results the following conclusions can be drawn.

1. For the heme-IX adducts, the non-interacting or interacting induced-dipole polarization energy represents 74% of the total energy MM2 + polarization. The electron-pair repulsion energy corresponds to 50% of the total energy MMX + polarization.
2. The model system takes into account the structural differences of the fixing centre in the Hb subunits. Certain conformations of heme IX–His models are much more favourable that others for fixing O_2.
3. Three different models of Fe-binding are proposed for O_2, CO and CN ligands: bent superoxide

Table 6. Selected geometric parameters (Å and degrees) from the geometry optimization of Fe(mdi)$_2$(py)(CN) with NLDFT [16][a]

Parameter	MM2	MM2 + NID[b]	MM2 + ID[c]	MMX[d]	MMX[d] + NID[b]	MMX[d] + ID[c]
Fe—$N_{porphyrin}$[e]	1.878	1.871	1.867	1.905	1.891	1.904
Fe—N_{Im}	1.868	1.860	1.858	2.022	1.964	2.036
Fe—C	1.944	1.942	1.941	2.079	2.032	2.064
C—N	1.164	1.163	1.164	1.211	1.217	1.216
Fe—C—N	179.8	179.8	179.6	176.2	177.1	177.3
Parameter		Experiment			NLDFT	
Fe—$N_{porphyrin}$		1.980			1.917	
Fe—N_{Im}		2.090			2.159	
Fe—C		1.930			1.903	
C—N		1.150			1.173	
Fe—C—N		180.0			180.0	

[a] Experimental data on the [Fe(OEP)(py)(CN)] system are also provided for comparison [68]; [b] NID: polarization by non-interacting induced dipoles; [c] ID: polarization by interacting induced dipoles; [d] Scaling factor $D = 0.1$; [e] Average values.

Fe^{III}—O_2^-, linear Fe^{II}—CO and linear Fe^{III}—CN^-. The nature of O_2 binding in Hb, Mb and simple Fe–porphyrin models is becoming clear. When O_2 is bound as a bent, rather than a triangular, ligand, it is best described as bound superoxide. This bent geometry may be critical to biological functioning because it allows the discrimination between O_2 and CO.

4. Rotations of Im and O_2 axial ligands about their linkages with Fe are unexpensive for both 5- and 6-coordinated systems. These rotations are practically free. A small modification of the model in both crystal and protein matrix affects the orientation of the ligands in experimental systems. In the structural minima the axial ligands are located about the bisector of an angle $N_{porphyrin}$—Fe—$N_{porphyrin}$.
5. The fact that in the present structure, a close analogue of the CO complexes of the hemoproteins, the Fe—C—O linkage is linear strongly suggests that another interpretation of the results of the protein studies is in order. The allegedly bent Fe—C—O linkage in these proteins is derived from Fourier maps on which the C and O atoms remain unresolved. These maps were interpreted on the assumption that the Fe—C vector is perpendicular to the porphyrin plane. It is much more reasonable to expect that owing to the fixed nature of the globin pocket bending will occur at the Fe atom, leading to a linear Fe—C—O bond, which is not perpendicular to the porphyrin plane.
6. The geometry optimizations performed on the experimental structures present a good agreement with the X-ray results, in spite of that only certain residues of the fixing centre have been taken into account. In oxy-Hb, His-distal is engaged in an H-bond with the O directly linked with Fe. The H-bond in the fixing centres of Hb differs from that customarily observed in the biomimetic systems and Mb, in which the H-bond is formed with the ending O. The electronic density of O(Fe) is lower than that of O(O), suggesting that the H-bond between O and His-distal is weaker than in Mb.

Acknowledgement

The author acknowledges financial support of the Spanish MCT (Plan Nacional I+D+I, Project No. BQU2001-2935-C02-01).

Appendix A. Force-field parameters

The MM2 parameter set (1980) has been used. Additional parameters are listed in Table A1. Type 13 is used for Fe.

Table A1. Additional MM2 parameters (Type 13 is used for Fe)

Angle	V_1	V_2	V_3		
Torsional Parameters					
1-1-2-7	−0.44	0.24	0.06		
1-1-2-9	−0.44	0.24	0.06		
5-1-2-7	0.0	0.0	−0.24		
5-1-2-9	0.0	0.0	−0.24		
1-2-2-9	0.0	10.0	0.0		
2-2-2-9	0.0	10.0	0.0		
5-2-2-9	0.0	10.0	0.0		
9-2-2-9	0.0	10.0	0.0		
1-2-6-24	0.0	0.0	0.0		
7-2-6-24	1.0	1.65	0.0		
1-2-9-2	0.0	10.0	0.0		
1-2-9-28	0.0	0.0	0.0		
2-2-9-2	0.0	10.0	0.0		
2-2-9-13	0.0	0.0	0.0		
2-2-9-28	0.0	0.0	0.0		
5-2-9-2	0.0	10.0	0.0		
5-2-9-13	0.0	0.0	0.0		
5-2-9-28	0.0	0.0	0.0		
9-2-9-2	0.0	10.0	0.0		
9-2-9-13	0.0	0.0	0.0		
7-4-13-9	0.0	0.0	0.0		
10-4-13-9	0.0	0.0	0.0		
7-7-13-9	0.0	0.0	0.0		
2-9-13-4	0.0	0.0	0.0		
2-9-13-7	0.0	0.0	0.0		
2-9-13-9	0.0	0.0	0.0		
Stretching parameters					
Bond	k_1	l_0	l_1	Bond moment	Fe oxidation state
4-7	10.0	1.110	0.0	0.089	2
4-7	10.0	1.158	0.0	0.010	3
4-13	10.0	1.968	0.0	−1.304	2
4-13	10.0	1.940	0.0	−1.374	3
7-7	10.0	1.210	0.0	0.000	3
7-13	10.0	1.841	0.0	−1.641	3
9-13	10.0	1.867	0.0	−1.514	2,3
Van der Waals parameters					
Atom	Type	R*	EPS	At. wt.	
13	Fe	0.013	2.912	55.85	
Bending parameters					
Angle	k_θ	θ_0			
1-2-7	0.5	120.0			
1-2-9	0.5	126.0			
2-2-9	0.5	108.0			
5-2-9	0.5	126.0			
6-2-7	0.5	120.0			
7-4-13	0.5	180.0			
10-4-13	0.5	180.0			
2-6-24	0.5	109.47122			
7-7-13	0.5	121.0			
2-9-2	0.5	108.0			
2-9-13	0.5	126.0			
4-13-9	0.0	109.47122			
7-13-9	0.0	109.47122			
9-13-9	0.0	109.47122			

Table A1. (Continued)

Out-of-plane bending parameters		
Angle	K_θ	θ_0
9-13	0.05	0.0
Stretching-bending parameters		
Parameter	$k_{l\theta}$	
1	0.0	
2	0.0	
3	0.0	
4	0.0	

References

1. M.F. Perutz: *Proc. R. Soc. London*, *B* **208**, 135 (1980).
2. M.F. Perutz, G. Fermi, B. Luisi, B. Shaanan, and R.C. Liddington: *Acc. Chem. Res.* **20**, 309 (1987).
3. K.G. Welinder: *Curr. Opin. Struct. Biol.* **2**, 388 (1992).
4. B.G. Malmström: *Chem. Rev.* **90**, 1247 (1990).
5. M. Sono, M.P. Roach, E.D. Coulter, and J.H. Dawson: *Chem. Rev.* **96**, 2841 (1996).
6. J. Barber and B. Andersson: *Nature* (*London*) **370**, 31 (1994).
7. C.L. Drennan, S. Huang, J.T. Drummond, R.G. Matthews, and M.L. Ludwig: *Science* **266**, 1669 (1994).
8. M.A. Halcrow and G. Christou: *Chem. Rev.* **94**, 2421 (1994).
9. M. Momenteau and C.A. Reed: *Chem. Rev.* **94**, 659 (1994).
10. A. Dedieu, M.-M. Rohmer, and A. Veillard: *Adv. Quantum Chem.* **16**, 43 (1982).
11. M.-M. Rohmer, A. Dedieu, and A. Veillard: *Chem. Phys.* **77**, 449 (1983).
12. M.-M. Rohmer: *Chem. Phys. Lett.* **116**, 44 (1985).
13. N. Li, Z. Su, P. Coppens, and J. Landrum: *J. Am. Chem. Soc.* **112**, 7294 (1990).
14. T.G. Spiro and P.M. Kozlowski: *J. Biol. Inorg. Chem.* **2**, 516 (1997).
15. T.G. Spiro and P.M. Kozlowski: *J. Am. Chem. Soc.* **120**, 4524 (1998).
16. T. Vangberg, D.F. Bocian, and A. Ghosh: *J. Biol. Inorg. Chem.* **2**, 526 (1997).
17. P. Jewsbury, S. Yamamoto, T. Minato, M. Saito, and T. Kitagawa: *J. Am. Chem. Soc.* **116**, 11586 (1994).
18. P. Jewsbury, S. Yamamoto, T. Minato, M. Saito, and T. Kitagawa: *J. Phys. Chem.* **99**, 12677 (1995).
19. A. Ghosh and D.F. Bocian: *J. Phys. Chem.* **100**, 6363 (1996).
20. E. Sigfridsson and U. Ryde: *J. Biol. Inorg. Chem.* **4**, 99 (1999).
21. C. Rovira, P. Ballone, and M. Parrinello: *Chem. Phys. Lett.* **271**, 247 (1997).
22. C. Rovira, K. Kunc, J. Hutter, P. Ballone, and M. Parrinello: *J. Phys. Chem. A* **101**, 8914 (1997).
23. C. Rovira, K. Kunc, J. Hutter, P. Ballone, and M. Parrinello: *Int. J. Quantum Chem.* **69**, 31 (1998).
24. C. Rovira and M. Parrinello: *Chem. Eur. J.* **5**, 250 (1999).
25. C. Rovira, P. Carloni, and M. Parrinello: *J. Phys. Chem. B* **103**, 7031 (1999).
26. R. Salzmann, M.T. McMahon, N. Godbout, L.K. Sanders, M. Wojdelski, and E. Oldfield: *J. Am. Chem. Soc.* **121**, 3818 (1999).
27. N. Godbout, L.K. Sanders, R. Salzmann, R.H. Havlin, M. Wojdelski, and E. Oldfield: *J. Am. Chem. Soc.* **121**, 3829 (1999).
28. G. Loew and M. Dupuis: *J. Am. Chem. Soc.* **118**, 10584 (1996).
29. D.L. Harris and G.H. Loew: *J. Am. Chem. Soc.* **118**, 10588 (1996).
30. D. Harris, G. Loew, and L. Waskell: *J. Am. Chem. Soc.* **120**, 4308 (1998).
31. D.E. Woon and G.H. Loew: *J. Phys. Chem. A* **102**, 10380 (1998).
32. O. Zakharieva, M. Grodzicki, A.X. Trautwein, C. Veeger, and I.M.C.M. Rietgens: *J. Biol. Inorg. Chem.* **1**, 192 (1996).
33. M.T. Green: *J. Am. Chem. Soc.* **120**, 10772 (1998).
34. G.B. Jameson, G.A. Rodley, W.T. Robinson, R.R. Gagne, C.A. Reed, and J.P. Collman: *Inorg. Chem.* **17**, 850 (1978).
35. G.B. Jameson, F.S. Molinaro, J.A. Ibers, J.P. Collman, J.I. Brauman, E. Rose, and K.S. Suslick: *J. Am. Chem. Soc.* **102**, 3224 (1980).
36. F. Maseras: *New J. Chem.* **22**, 327 (1998).
37. J.-D. Maréchal, G. Barea, F. Maseras, A. Lledós, L. Mouawad, and D. Pérahia: *J. Comput. Chem.* **21**, 282 (2000).
38. R. Salzmann, C.J. Ziegler, N. Godbout, M.T. McMahon, K.S. Suslick, and E. Oldfield: *J. Am. Chem. Soc.* **120**, 11323 (1998).
39. S. Han, K. Cho, and J. Ihm: *Phys. Rev. E* **59**, 2218 (1999).
40. K. Kim, J. Fettinger, J.L. Sessler, M. Cyr, J. Hugdahl, J.P. Collman, and J.A. Ibers: *J. Am. Chem. Soc.* **111**, 403 (1989).
41. M.P. Johansson, M.R.A. Blomberg, D. Sundholm, and M. Wikström: *Biochim. Biophys. Acta* **1553**, 183 (2002).
42. M.P. Johansson, D. Sundholm, G. Gerfen, and M. Wikström: *J. Am. Chem. Soc.* **124**, 11771 (2002).
43. F. Torrens, M. Ruiz-López, C. Cativiela, J.I. García, and J.A. Mayoral: *Tetrahedron* **48**, 5209 (1992).
44. F. Torrens: *Mol. Simul.* **24**, 391 (2000).
45. N.L. Allinger: *J. Am. Chem. Soc.* **99**, 8127 (1977).
46. F. Torrens: *Polyhedron* **22**, 1091 (2003).
47. B.T. Thole: *Chem. Phys.* **59**, 341 (1981).
48. T.L. Hill: *J. Chem. Phys.* **16**, 399 (1948).
49. J.A. Deiters, J.C. Gallucci, T.E. Clark, and R.R. Holmes: *J. Am. Chem. Soc.* **99**, 5461 (1977).
50. H. Yow and L.S. Bartell: *J. Mol. Struct.* **15**, 209 (1973).
51. F. Torrens: *J. Phys. Org. Chem.* **15**, 742 (2002).
52. R.S. Mulliken: *J. Chem. Phys.* **2**, 782 (1934).
53. J.E. Huheey: *J. Phys. Chem.* **69**, 3284 (1965).
54. R.T. Sanderson: *Science* **114**, 670 (1951).
55. R.S. Mulliken, C.A. Rieke, D. Orloff, and H. Orloff: *J. Chem. Phys.* **17**, 1248 (1949).
56. C. Joachim, G. Treboux, and H. Tang: A model conformational flip-flop molecular switch. In *Molecular Electronics: Science and Technology*, AIP Conference Proceedings Vol. 262, AIP, New York (1992), pp. 107–117.
57. A.I. Vogel: *J. Chem. Soc.* 1833 (1948).
58. N. Gresh, P. Claverie, and A. Pullman: *Int. J. Quantum Chem. Symp.* **13**, 243 (1979).
59. A.K. Rappé, C.J. Casewit, K.S. Colwell, W.A. Goddard III, and W.M. Skiff: *J. Am. Chem. Soc.* **114**, 10024 (1992).
60. M. Momenteau, W.R. Scheidt, C.W. Eigenbrot, and C.A. Reed: *J. Am. Chem. Soc.* **110**, 1207 (1988).
61. J.J. Weiss: *Nature* (*London*) **202**, 83 (1964).
62. H.P. Misra and I. Fridovich: *J. Biol. Chem.* **247**, 6960 (1972).
63. L. Pauling: *Proc. Natl. Acad. Sci. USA* **74**, 2612 (1977).
64. M.J.S. Dewar, E.G. Zoebisch, E.F. Healy, and J.J.P. Stewart: *J. Am. Chem. Soc.* **107**, 3902 (1985).
65. R. Huber, O. Epp, and H. Formanek: *J. Mol. Biol.* **52**, 349 (1970).
66. E.A. Padian and W.E. Love: *J. Biol. Chem.* **249**, 4067 (1974).
67. J.C. Norvell, A.C. Nunes, and B.P. Schoenborn: *Science* **190**, 568 (1975).
68. W.R. Scheidt and K. Hatano: *Acta Crystallogr. Sect. C* **47**, 2201 (1991).